doi:10.1038/nature06907

LETTERS

The Cl^-/H^+ antiporter ClC-7 is the primary chloride permeation pathway in lysosomes

Austin R. Graves[1], Patricia K. Curran[1], Carolyn L. Smith[2] & Joseph A. Mindell[1]

Lysosomes are the stomachs of the cell—terminal organelles on the endocytic pathway where internalized macromolecules are degraded. Containing a wide range of hydrolytic enzymes, lysosomes depend on maintaining acidic luminal pH values for efficient function. Although acidification is mediated by a V-type proton ATPase, a parallel anion pathway is essential to allow bulk proton transport[1,2]. The molecular identity of this anion transporter remains unknown. Recent results of knockout experiments raise the possibility that ClC-7, a member of the CLC family of anion channels and transporters, is a contributor to this pathway in an osteoclast lysosome-like compartment, with loss of ClC-7 function causing osteopetrosis[3]. Several mammalian members of the CLC family have been characterized in detail; some (including ClC-0, ClC-1 and ClC-2) function as Cl^--conducting ion channels[4], whereas others act as Cl^-/H^+ antiporters (ClC-4 and ClC-5)[5,6]. However, previous attempts at heterologous expression of ClC-7 have failed to yield evidence of functional protein, so it is unclear whether ClC-7 has an important function in lysosomal biology, and also whether this protein functions as a Cl^- channel, a Cl^-/H^+ antiporter, or as something else entirely. Here we directly demonstrate an anion transport pathway in lysosomes that has the defining characteristics of a CLC Cl^-/H^+ antiporter and show that this transporter is the predominant route for Cl^- through the lysosomal membrane. Furthermore, knockdown of ClC-7 expression by short interfering RNA can essentially ablate this lysosomal Cl^-/H^+ antiport activity and can strongly diminish the ability of lysosomes to acidify *in vivo*, demonstrating that ClC-7 is a Cl^-/H^+ antiporter, that it constitutes the major Cl^- permeability of lysosomes, and that it is important in lysosomal acidification.

We pursued the function of ClC-7 by using biochemical methods to characterize the Cl^- permeability properties of native lysosomal membranes. We isolated lysosomes from rat liver by using differential sedimentation through a Percoll gradient[7]. This preparation is strongly enriched for LAMP-1, a lysosomal marker, and is strongly depleted for markers of plasma membranes, endosomes, endoplasmic reticulum and mitochondria (Supplementary Fig. 1), suggesting that subsequent functional observations represent transport in lysosomes. We focused on Cl^- transport pathways in these experiments, inhibiting H^+-ATPases by including no ATP outside the lysosomes.

To assess Cl^- transport, we used the concentrative uptake method[8,9]. Lysosomes loaded with a high concentration of unlabelled Cl^- were diluted into a buffer containing a trace amount of $^{36}Cl^-$. If these organelles contain a specific electrogenic transport pathway for Cl^-, they will concentrate the labelled Cl^- inside. Indeed, we observed rapid uptake of $^{36}Cl^-$, abolished by addition of the K^+ ionophore valinomycin (Fig. 1a, open symbols), indicating a specific electrogenic pathway for the ion (Fig. 1a). (The falling phase of $^{36}Cl^-$ uptake after 15 s probably represents small leaks of ions through other transport pathways, which dissipate the large transmembrane voltage in these native lysosomes.) Varying internal anions in similar experiments reveals the following apparent permeability sequence: $CH_3SO_3^- < I^- \ll Cl^- \approx Br^- < NO_3^-$ (Fig. 1b). Reduced uptake with I^- inside the lysosomes (Fig. 1b) is reminiscent of the effects of this ion on many CLC family members, which have a low I^- conduction[10–12]. Uptake was enhanced at pH 4.0 for all permeable ions tested (Fig. 1a, b), which is consistent with activity at physiological lysosomal pH.

pH-dependent concentrative Cl^- uptake could arise either from pH-modulated conduction through an ion channel or from acid activation of a Cl^-/H^+ antiporter. To distinguish between these possibilities we assayed lysosomes for $^{36}Cl^-$ uptake in symmetrical $[Cl^-]$ but in the presence of a pH gradient ($[H^+]_{in} > [H^+]_{out}$). In these conditions, a pH gradient will drive the accumulation of $^{36}Cl^-$ only if the movement of Cl^- is coupled to that of protons. High levels of $^{36}Cl^-$ uptake (Fig. 1c, filled symbols), abolished by collapsing the pH gradient with the proton ionophore carbonyl cyanide 4-(trifluoromethoxy)phenylhydrazone (FCCP; open symbols), show the presence of coupled Cl^-/H^+ antiport.

To explore the coupling between Cl^- and H^+ gradients further, we monitored the effects of a Cl^- gradient on the intralysosomal pH by attempting to drive protons uphill with a Cl^- gradient while monitoring internal pH with the ratiometric fluorophore 2′,7′-bis-(2-carboxyethyl)-5(6)-carboxyfluorescein (BCECF). The internal pH is stable until valinomycin is added to initiate transport (Fig. 2a, grey arrow). Ensuing alkalinization (red trace) reflects protons being driven out of the lysosomes against their pH gradient, confirming functional Cl^-/H^+ antiport. Subsequent addition of 1 μM FCCP (asterisks) collapses the proton gradient. Control experiments exclude the possibility of a significant proton leak in these conditions (Supplementary Fig. 2).

We distinguished indirect (separate protein pathways for H^+ and Cl^-) from direct coupling mechanisms (obligate antiport of both ions through a common transporter) by measuring the equilibrium potential for H^+ flux, monitoring this flux with BCECF at a series of voltages set with K^+/valinomycin. Whereas at 0 mV (Fig. 2a, red trace) the internal pH increases on the addition of valinomycin, at −92 mV (dark blue trace, same H^+/Cl^- gradients) the internal pH decreases. Similar measurements at a series of voltages identify the potential at which there is no net H^+ flux (Fig. 2a, green trace, and Fig. 2b). This reversal potential represents thermodynamic equilibrium and can be compared with predictions based on uncoupled H^+ transport (E_H) as well as with possible stoichiometries of Cl^-/H^+ antiport calculated with the antiporter equation[13] (E_{trans}). For the conditions examined in Fig. 2a, an uncoupled H^+ transporter would be predicted to have a reversal potential of +12 mV, the Nernst

[1]Membrane Transport Biophysics Unit, and [2]Light Microscopy Facility, Porter Neuroscience Research Center, National Institute of Neurological Disorders and Stroke, National Institutes of Health, 35 Convent Drive, Building 35, MSC 3701, Bethesda, Maryland 20892, USA.

potential for H^+ (E_H, lower pink arrow in Fig. 2b). In contrast, a coupled Cl^-/H^+ antiporter would be predicted to show flux reversal at −54, −47 or −32 mV (upper pink and red arrows in Fig. 2b) depending on its relative stoichiometry for Cl^- and H^+. The measured reversal potential is clearly far from that of an uncoupled pathway (Fig. 2b) and agrees well with the predicted reversal potential for a fixed stoichiometry of $2Cl^-:1H^+$. A very different set of ionic conditions (symmetrical Cl^- and a 1-unit pH gradient) similarly yields a reversal potential consistent with a $2Cl^-:1H^+$ stoichiometry (Fig. 2b, blue data and arrows). Thus, the lysosomal transport of Cl^- and H^+ reflects thermodynamically coupled transport through a common protein, a Cl^-/H^+ antiporter with a 2:1 coupling ratio, which provides the major proton pathway in the lysosome (other than the H^+-ATPase, which is inactive in these experiments).

However, our proton flux measurements do not reveal whether the Cl^-/H^+ antiporter is the major pathway for chloride through lysosomal membranes or is one of several molecular routes for this anion. We can nevertheless assess the contribution of the antiporter to the total Cl^- conductance of lysosomes by measuring the reversal potential for Cl^- flux into these organelles. We monitored lysosomal Cl^- concentration changes with 6-methoxy-*N*-(3-sulphopropyl)quinolinium, inner salt (SPQ), a well-studied fluorescent probe that is effectively quenched by Cl^- (ref. 14). Even though SPQ fluorescence is known to depend somewhat on pH, control experiments (data not shown) reveal the fluorophore to be minimally pH-dependent in the range of ΔpH measured here. We trapped SPQ in lysosomes and measured changes in fluorescence emission on the addition of valinomycin (Fig. 2c). Depending on the membrane voltage (V_m), a single set of Cl^- and H^+ gradients can result in Cl^- efflux ($V_m = -59$ mV; Fig. 2c, upper left), influx ($V_m = -18$ mV or +20 mV; Fig. 2c, lower left and lower right) or nearly undetectable flux ($V_m = -25$ mV, Fig. 2c, upper right). By plotting the integral of the difference between initial and final spectra at these voltages, we can estimate the reversal potential for Cl^- flux (Fig. 2d). The measured reversal potential should be the weighted mean of the reversal potentials for each transporter or channel actively conducting Cl^-, reflecting the relative contribution of each permeation pathway to the total flux. The observed flux reverses at about –25 mV, very near the predicted reversal potential of a $2Cl^-:1H^+$ antiporter (Fig. 2d), showing that the vast majority of lysosomal Cl^- flux is through the Cl^-/H^+ antiporter. In combination, the characteristics of this transporter—2:1 Cl^-/H^+ antiport, acid activation, and reduced uptake in I^-—strongly suggest that it is a member of the CLC family.

Which CLC could be the lysosomal Cl^-/H^+ antiporter? Western blots reveal that rat liver expresses the following: ClC-2; at least one of ClC-3, ClC-4 and ClC-5; ClC-6; and ClC-7 (Fig. 3a). Of these CLCs, only ClC-7 is highly enriched in our lysosomes—strongly contrasting with the others, which were all markedly depleted. Thus, ClC-7 is a prime candidate for the lysosomal antiporter, a function consistent with its role in osteopetrosis[3,15–17] and in lysosomal storage disease[18].

To establish a molecular connection between ClC-7 and the lysosomal antiporter conclusively, we performed gene-specific knockdown (short interfering RNA (siRNA)) experiments in HeLa cells. These cells express lysosome-localized ClC-7 (Fig. 3a and Supplementary Figs 1 and 4) and possess similar lysosomal Cl^-/H^+ antiport activity to that of rat liver lysosomes (Fig. 3c, black trace, and Supplementary Fig. 5). We knocked down ClC-7 expression with siRNAs directed against two non-overlapping sequences from the gene. With a single transfection of siRNA these cells show somewhat decreased levels of the ClC-7 protein on western blots (Fig. 3b) and show modest, but significant, decreases in H^+-driven $^{36}Cl^-$ uptake in comparison with untransfected HeLa cells (Fig. 3c; for siRNA 1, $P = 0.0070$; for siRNA2, $P = 0.0092$). Prolonging exposure to the siRNA with two sequential transfections resulted in near-complete knockdown of ClC-7 protein levels (Fig. 3b) as well as near-total loss of H^+-driven $^{36}Cl^-$ uptake (Fig. 3c, red diamonds; $P = 7 \times 10^{-6}$). Uptake and protein levels were essentially unaffected in HeLa cells transfected with random, scrambled siRNA (Fig. 3a–c). Thus, the ClC-7 protein accounts for essentially all of the observed Cl^-/H^+ antiport activity, which is definitive evidence that ClC-7 is the Cl^-/H^+ antiporter expressed in lysosomes.

If ClC-7 constitutes the long-sought voltage shunt in the lysosomal membrane, disrupting its function would be expected to interfere with lysosomal acidification *in vivo*. We tested this prediction by staining live wild-type (WT) and ClC-7 knockdown HeLa cells with LysoTracker Green, a weakly basic fluorescent probe that stains organelles by virtue of their acidity. We reasoned that if knocking down ClC-7 protein levels affects lysosomal acidification, the knockdown cells should stain less strongly with a LysoTracker dye. Even though LysoTracker may also stain other acidic compartments, any significant disruption in lysosomal acidification should be apparent using this approach. ClC-7 knockdown cells show no gross morphological abnormalities (Fig. 4a, top row). When stained with LysoTracker Green, both WT and control HeLa cells showed dense staining with many punctate objects, presumably lysosomes (Fig. 4a, confocal slice; row 2). In contrast, most ClC-7 knockdown cells showed only a few such puncta, although in every experiment we observed occasional cells with staining comparable to that in the controls (see, for example, Fig. 4a, arrow); these cells may not have been successfully transfected with siRNA, providing a useful control for the imaging conditions. Integrating the total summed intensity from confocal stacks of individual cells (Fig. 4a, row 3) provides a quantitative measure of staining (Fig. 4c) and reveals a significant decrease in ClC-7 knockdown cells compared with either WT ($P = 7.7 \times 10^{-5}$)

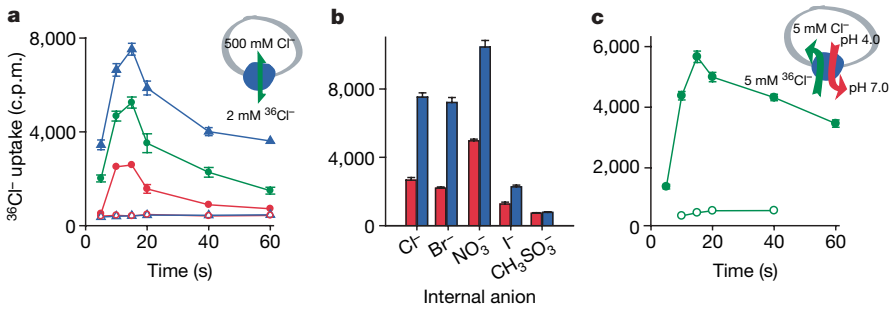

Figure 1 | $^{36}Cl^-$ flux in native rat liver lysosomes. **a**, Concentrative uptake by lysosomes. Lysosomes containing 500 mM KCl, pH 7.0 (red), pH 5.5 (green) or pH 4.0 (blue) were added to a solution containing 2 mM $Na^{36}Cl$ at the same pH at $t = 0$ without (filled symbols) or with (open symbols) 1 μM valinomycin. Reactions were stopped at the indicated times and retained radioactivity was measured. **b**, Ion dependence of concentrative uptake. Experiments were performed as above, but with internal Cl^- replaced by the indicated anions; the bars represent $^{36}Cl^-$ uptake at the 20-s time point at pH 7.0 (red bars) or pH 4.0 (blue bars). **c**, Proton-driven $^{36}Cl^-$ uptake. Experiments were performed as above but with symmetrical Cl^- and a proton driving force (5 mM NaCl at pH 4.0 inside and 5 mM $Na^{36}Cl$ at pH 7.0 with 1 μM valinomycin outside). Data are shown in the absence (closed symbols) or presence (open symbols) of 1 μM FCCP. See Methods for other solution details. $n = 3$–6; error bars represent s.e.m. and are not shown if they are smaller than the symbols.

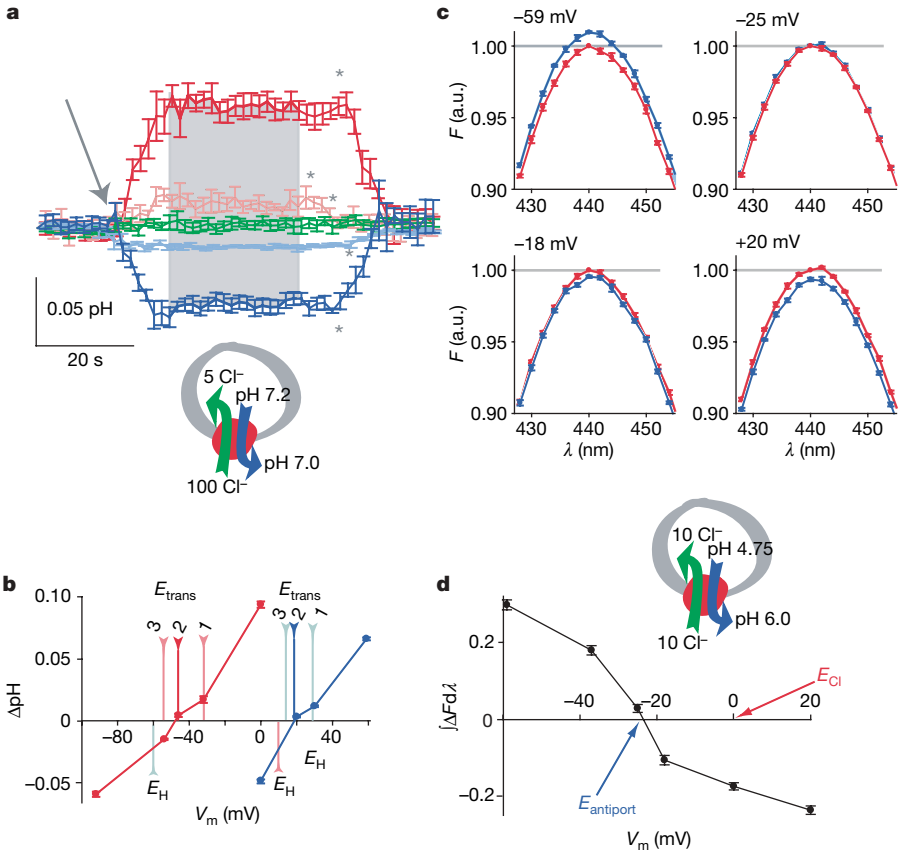

Figure 2 | Fluorescence monitoring of lysosomal H^+ and Cl^- flux. **a**, Cl^--driven proton movement. ΔpH was measured with the ratiometric BCECF signal (see Methods). $[Cl^-]_{in}$ = 5 mM, pH_{in} = 7.2; $[Cl^-]_{out}$ = 100 mM, pH_{out} = 7.0, $[K^+_{out}]$ = 5 mM. Internal K^+ concentration was varied to set E_K at 0 mV (red trace), −32 mV (pink trace), −46 mV (green trace), −56 mV (light blue trace) or −92 mV (dark blue trace). The addition of 1 μM valinomycin initiated transport (arrow). Experiments were terminated by the addition of FCCP (asterisk). n = 5–8; error bars represent s.e.m. **b**, Reversal potentials of Cl^--driven proton transport. Steady-state ΔpH from two sets of conditions: red symbols represent data from **a**; blue symbols represent $[Cl^-]_{in} = [Cl^-]_{out}$ = 10 mM, pH_{in} = 6.0, pH_{out} = 5.0. Red (pH 7.0/7.2) and blue (pH 5.0/6.0) arrows below the x axis indicate predicted reversal potentials for an uncoupled transporter (E_H). Arrows above the x axis indicate predicted reversal potentials for coupled Cl^-/H^+ antiport ($3Cl^-$:$1H^+$ (3), $2Cl^-$:$1H^+$ (2) or $1Cl^-$:$1H^+$ (1)). Each point represents the mean ± s.e.m. of 13–15 steady-state points (grey area in **a**) from each of five to eight experiments. **c**, Baseline emission spectra at indicated voltages (red symbols, normalized to 1.00 at 440 nm, grey line) with 10 mM Cl^-, pH 4.75 inside lysosomes and 10 mM Cl^-, pH 6.0 outside; the addition of 1 μM valinomycin initiated Cl^- flux; after 2 min a second spectrum was obtained (blue symbols). **d**, Reversal potential for Cl^- flux: each point represents the integrated difference spectrum at the given voltage (area between spectra in **c**). The arrows indicate E_{Cl} (red) and $E_{2:1}$ (blue, the predicted reversal potential for a 2:1 Cl^-/H^+ antiporter). n = 4–6; error bars represent s.e.m.

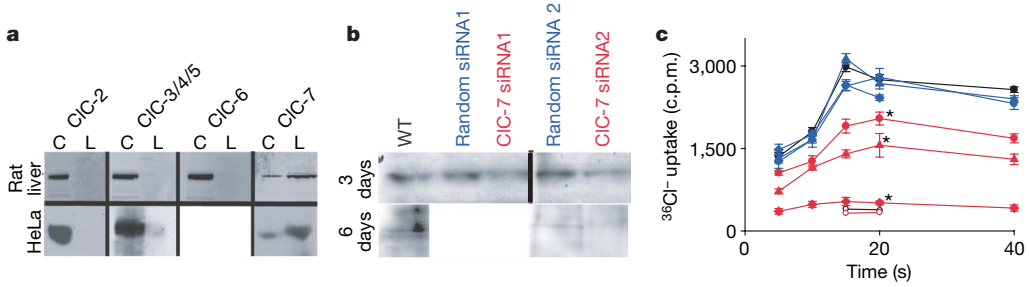

Figure 3 | ClC-7 mediates lysosomal Cl^-/H^+ antiport. **a**, Western blots of CLCs in rat liver and HeLa cells. For each CLC shown, blots indicate expression levels in crude lysate (C) and the lysosome-enriched fraction (L). The antibody against the ClC-3/4/5 subfamily cross-reacts with all three members of that group. No ClC-6 expression was observed in HeLa cells. **b**, Western blots of ClC-7 in whole-cell lysates of HeLa cells either untransfected (WT) or transfected with either random non-coding siRNA or with one of two different ClC-7-specific siRNAs. Cells were transfected with either a three-day single-stage protocol or a six-day two-stage protocol (see Methods for details). The conditions used for the three-day and six-day blots were different; WT controls are included in both cases as references for baseline ClC-7 expression. **c**, H^+-driven $^{36}Cl^-$ uptake in lysosomes isolated from WT HeLa cells (filled black symbols), three different preparations of HeLa cells transfected with control siRNA (filled blue symbols; circles and triangles represent single transfection, diamonds represent double transfection) or HeLa cells transfected with two different ClC-7-specific siRNAs (filled red triangles, filled red circles and filled red diamonds). For one of the ClC-7 siRNAs, data are shown for both a single siRNA transfection (red triangles) and a two-stage transfection (red diamonds; see Methods for details). FCCP controls are shown at two time points for WT (open black symbols) and one ClC-7 siRNA (open red symbols). Asterisks indicate statistically significant differences compared with WT (siRNA1, 3 days: P = 0.0092; siRNA2, 3 days: P = 0.0070; siRNA2, 6 days: $P = 7 \times 10^{-6}$; two-tailed Student's t-test). n = 3; error bars represent s.e.m.

or control-siRNA-transfected ($P = 3.3 \times 10^{-9}$) HeLa cells. (Note that the control-siRNA-transfected cells show a marginal increase in LysoTracker staining.) When stained with an anti-LAMP-1 antibody, WT, siRNA control and ClC-7 siRNA cells showed similar staining patterns (Fig. 4b), suggesting that lysosomes still exist in the ClC-7 knockdown cells. In combination with the results above, which point to a specific lysosomal effect of ClC-7 knockdown, these results demonstrate that a decrease in ClC-7 *in vivo* compromises lysosomal acidification and support our conclusion that this transporter represents the major pathway for Cl^- in this organelle.

We have established that ClC-7 is a Cl^-/H^+ antiporter, revealing that the last remaining uncharacterized subfamily of CLCs consists of antiporters rather than ion channels. This leads to the general conclusion that for CLCs, subcellular localization correlates strictly with function; the two subfamilies of intracellular CLCs are both proton-coupled Cl^- transporters, whereas the plasma-membrane CLCs are all ion channels. Our results establish the stoichiometry of ClC-7 as $2Cl^-:1H^+$; they are in agreement with the approximate measurements already made for ClC-4 and ClC-5 (refs 5, 6) and with the measurement for the plant antiporter AtClCa (ref. 19), supporting the contention that the basic mechanism of antiport is conserved between bacterial, plant and mammalian CLC transporters.

The present results have functional implications for the cell biology of the lysosome, because ClC-7 accounts for the major anion pathway of this organelle. Previous results have shown that lysosomal acidification depends on the presence of external Cl^- (refs 1, 2); our knockdown experiments reveal that this pathway is essential for the lysosomal acidification mechanism. Although the existence of such a pathway has long been inferred[1], its molecular identity is now clear. A series of CLC antiporters participate in acidification in the endosomal pathway, with ClC-4 and ClC-5 involved in early endosomes, ClC-6 localizing to late endosomes, and ClC-7 involved in lysosomes[20]. These compartments have progressively more acidic interiors; because they express the same H^+-ATPase, we speculate that cells vary the identity of the CLC transporter to help in determining the final pH setpoint of each organelle in the endocytic pathway. Because a loss of ClC-7 function leads to osteopetrosis, it has been suggested that a ClC-7 inhibitor could serve as a treatment for osteoporosis[21]; the functional assay system described here could be of use in high-throughput screening for such inhibitors.

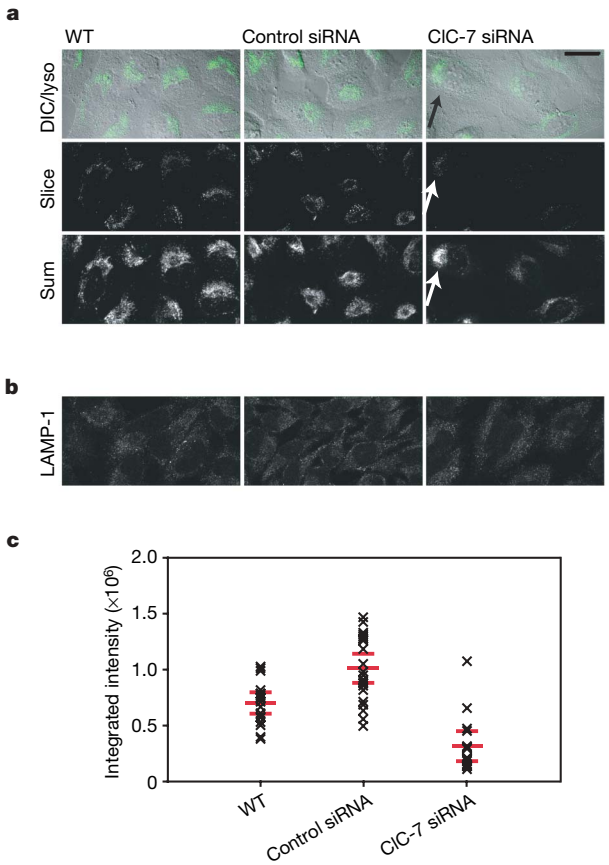

Figure 4 | ClC-7 is essential for lysosomal acidification *in vivo*. **a**, Confocal images of live WT, control-siRNA-transfected and ClC-7-siRNA-transfected HeLa cells stained with LysoTracker Green dye. Top row, differential interference contrast images overlaid with summed LysoTracker intensity (green); middle row, the brightest single confocal slice from the LysoTracker Green channel for the same field; bottom row, summed Lysotracker Green intensity for all confocal slices through the total thickness of the field. The arrows indicate a cell in the ClC-7 knockdown condition with a LysoTracker staining level roughly the same as that of the WT. **b**, Confocal images of WT, control-siRNA-transfected and ClC-7-siRNA-tranfected HeLa cells fixed and stained with anti-LAMP-1 antibody. **c**, Integrated LysoTracker Green staining intensity of summed slices through WT, control-siRNA-transfected and ClC-7-siRNA-transfected HeLa cells. The intensity for each measured cell is denoted by a cross, with the mean being indicated by a long red bar; s.e.m. is denoted by short red bars. Differences between ClC-7-siRNA-transfected and WT cells and between ClC-7-siRNA-transfected and control-siRNA-transfected cells were significant ($P = 7.7 \times 10^{-5}$ and 3.3×10^{-9}, respectively). Scale bar, 29 μm. Each row of images in **a** and **b** was collected with identical imaging settings and was processed identically.

METHODS SUMMARY

Lysosomal enrichment from rat liver and HeLa cell culture. Saline-perfused rat livers were homogenized with a motorized Potter–Elvehjem homogenizer. Lysosomes were isolated by differential centrifugation on a Percoll gradient[7] and fractions were identified with enzyme assays or western blots with anti-LAMP-1 antibody.

Concentrative and proton-driven $^{36}Cl^-$ uptake. Lysosomal samples containing 100 μg of total protein were loaded by freeze–thawing followed by sonication in the desired buffer, and external solutions were exchanged by using Sephadex G-50 columns equilibrated in external buffer. Concentrative uptake was initiated by adding 2 mM $^{36}Cl^-$ to the outside buffer; proton-driven $^{36}Cl^-$ uptake was initiated by the addition of 1 μM valinomycin to the outside buffer. Reactions were terminated by filter binding and radioactivity was measured by liquid scintillation.

Fluorescence measurements of H^+ and Cl^- flux. BCECF or SPQ (200 μM) was trapped in lysosomes along with internal solution by freeze–thawing followed by sonication; external solutions were replaced as above. Lysosomes were introduced to a Jobin–Yvon Fluoromax-3 fluorimeter and stirred at 22 °C. BCECF excitation wavelengths alternated between 500 and 450 nm; emission was measured at 535 nm. SPQ was excited at 344 nm; emission spectra (420–460 nm) were collected. Transport was initiated by adding 1 μM valinomycin.

Cell culture and siRNA-mediated knockdown of ClC-7. HeLa cells were grown to generate a harvest of about 6 g of cells for lysosome preparations or on chambered coverglasses for imaging. Cells were transfected with 46 nM siRNA complexed with siPORT NeoFx (Ambion) and either collected at 72 h (single transfection) or re-transfected for a further 72 h (double transfection). Collected cells were lysed by using nitrogen cavitation[22], and lysosomes were prepared as above. The siRNA sequences used were as follows: ClC-7 siRNA1, GGCCUCAUCAACUUCGGAAtt (104370; Ambion); ClC-7 siRNA2, CCUCUCCGAGUUCAUGAACtt (145731; Ambion).

Imaging of HeLa cells. Cells were imaged with a Zeiss LSM 510 confocal microscope after 10 min in 50 nM LysoTracker Green (Invitrogen). Similar results were obtained for at least four transfections. For immunostaining, fixed cells were stained with anti-LAMP-1 primary antibody and an Alexa-546 conjugated secondary antibody.

Received 28 September 2007; accepted 10 March 2008.
Published online 30 April 2008.

1. Dell'Antone, P. Evidence for an ATP-driven 'proton pump' in rat liver lysosomes by basic dyes uptake. *Biochem. Biophys. Res. Commun.* **86**, 180–189 (1979).
2. Ohkuma, S., Moriyama, Y. & Takano, T. Identification and characterization of a proton pump on lysosomes by fluorescein-isothiocyanate-dextran fluorescence. *Proc. Natl Acad. Sci. USA* **79**, 2758–2762 (1982).
3. Kornak, U. *et al.* Loss of the ClC-7 chloride channel leads to osteopetrosis in mice and man. *Cell* **104**, 205–215 (2001).
4. White, M. M. & Miller, C. A voltage-gated anion channel from the electric organ of *Torpedo californica*. *J. Biol. Chem.* **254**, 10161–10166 (1979).

5. Picollo, A. & Pusch, M. Chloride/proton antiporter activity of mammalian CLC proteins ClC-4 and ClC-5. *Nature* **436,** 420–423 (2005).
6. Scheel, O., Zdebik, A. A., Lourdel, S. & Jentsch, T. J. Voltage-dependent electrogenic chloride/proton exchange by endosomal CLC proteins. *Nature* **436,** 424–427 (2005).
7. Graham, J. M. in *Current Protocols in Cell Biology* (eds Bonifacino, J. S., Dasso, M., Harford, J. B., Lippincott-Schwartz, J. & Yamada, K. M.) 3.6.1–3.6.21 (Wiley, Hoboken, NJ, 2000).
8. Goldberg, A. F. & Miller, C. Solubilization and functional reconstitution of a chloride channel from *Torpedo californica* electroplax. *J. Membr. Biol.* **124,** 199–206 (1991).
9. Garty, H., Rudy, B. & Karlish, S. J. A simple and sensitive procedure for measuring isotope fluxes through ion-specific channels in heterogenous populations of membrane vesicles. *J. Biol. Chem.* **258,** 13094–13099 (1983).
10. Rychkov, G. Y., Pusch, M., Roberts, M. L., Jentsch, T. J. & Bretag, A. H. Permeation and block of the skeletal muscle chloride channel, ClC-1, by foreign anions. *J. Gen. Physiol.* **111,** 653–665 (1998).
11. Jentsch, T. J., Friedrich, T., Schriever, A. & Yamada, H. The CLC chloride channel family. *Pflugers Arch.* **437,** 783–795 (1999).
12. Maduke, M., Pheasant, D. J. & Miller, C. High-level expression, functional reconstitution, and quaternary structure of a prokaryotic ClC-type chloride channel. *J. Gen. Physiol.* **114,** 713–722 (1999).
13. Accardi, A. & Miller, C. Secondary active transport mediated by a prokaryotic homologue of ClC Cl^- channels. *Nature* **427,** 803–807 (2004).
14. Illsley, N. P. & Verkman, A. S. Membrane chloride transport measured using a chloride-sensitive fluorescent probe. *Biochemistry* **26,** 1215–1219 (1987).
15. Henriksen, K. *et al.* Characterization of osteoclasts from patients harboring a G215R mutation in ClC-7 causing autosomal dominant osteopetrosis type II. *Am. J. Pathol.* **164,** 1537–1545 (2004).
16. Letizia, C. *et al.* Type II benign osteopetrosis (Albers-Schonberg disease) caused by a novel mutation in CLCN7 presenting with unusual clinical manifestations. *Calcif. Tissue Int.* **74,** 42–46 (2004).
17. Kornak, U., Ostertag, A., Branger, S., Benichou, O. & de Vernejoul, M. C. Polymorphisms in the CLCN7 gene modulate bone density in postmenopausal women and in patients with autosomal dominant osteopetrosis type II. *J. Clin. Endocrinol. Metab.* **91,** 995–1000 (2006).
18. Kasper, D. *et al.* Loss of the chloride channel ClC-7 leads to lysosomal storage disease and neurodegeneration. *EMBO J.* **24,** 1079–1091 (2005).
19. De Angeli, A. *et al.* The nitrate/proton antiporter AtCLCa mediates nitrate accumulation in plant vacuoles. *Nature* **442,** 939–942 (2006).
20. Jentsch, T. J. Chloride and the endosomal–lysosomal pathway: emerging roles of CLC chloride transporters. *J. Physiol. (Lond.)* **578,** 633–640 (2007).
21. Schaller, S. *et al.* The chloride channel inhibitor NS3736 prevents bone resorption in ovariectomized rats without changing bone formation. *J. Bone Miner. Res.* **19,** 1144–1153 (2004).
22. Gottlieb, R. A. & Adachi, S. Nitrogen cavitation for cell disruption to obtain mitochondria from cultured cells. *Methods Enzymol.* **322,** 213–221 (2000).

Supplementary Information is linked to the online version of the paper at www.nature.com/nature.

Acknowledgements We thank K. Swartz, M. Maduke, J. Diamond and R. Youle for critical readings of the manuscript; R. Brady, G. Murray and R. Puertollano-Moro for advice on lysosomes; and the members of the Mindell laboratory for discussions. This work was supported by the NINDS intramural program.

Author Information Reprints and permissions information is available at www.nature.com/reprints. Correspondence and requests for materials should be addressed to J.A.M. (mindellj@ninds.nih.gov).

Supplemental Results

Stability of pH in lysosomes

Since our quantitative measurements of antiporter stoichiometry require well-controlled and stable internal lysosomal pH, we performed experiments to measure this in the absence of antiport (no valinomycin added). Good control of the lysosomal pH is particularly critical when we are measuring reversal potential (Figure 2), since these quantitative measurements are compared with theoretical predictions which incorporate the pH. For the experimental conditions of the proton reversal potential measurements we could measure pH stability directly. Rather than initiating antiport after 15 s (by adding valinomycin, Supplemental Figure 2A, red arrow and red trace), we waited ~150 seconds (brown arrow, brown trace) during which time we would expect to observe a change in pH if the lysosomes have a proton leak. The pH is clearly stable over this time period, which is longer than the duration of the experiments in Figure 2, demonstrating that there is no significant proton leak in the lysosomal membrane in parallel to the antiporter under these conditions. The value of initial pH for these experiments (averaged over 120 s) was 7.18 ± 0.03 (mean ± s.e.m., N = 3) indicating that the actual pH inside the lysosomes was near the desired value of 7.20. We also sought to verify that the pH is stable inside the lysosomes under the ionic conditions used to measure Cl^- reversal potential, where they must withstand a larger, 1.25 unit, pH gradient. However, the internal pH for these experiments was 4.75, far from the usual working range of BCECF. Control experiments with BCECF free in solution (Supplemental Figure 3) reveal that there is a discontinuity in the pH-dependence of the fluorophore, around pH 5.25, below which the it is no longer significantly pH sensitive (Supplemental Figure 3). Therefore we measured the pH stability of lysosomes at a slightly higher internal pH (5.5) while maintaining either a 1 unit (pH 6.5 outside, Supplemental Figure 2b, green trace) or a 2 unit gradient (pH 7.5 outside, Supplemental Figure 2b, blue trace). In either condition the internal pH of the lysosomes is stable over 150 s, again longer than the time scale of the relevant experiment. In both cases, addition of valinomycin initiates a pH change which reflects antiporter activity, with a larger flux caused by the larger pH gradient as expected. In these experiments the initial pH was 5.56 ± 0.00 (mean ± s.e.m., N=3), again indicating that the actual pH is near the intended pH (of pH 5.50).

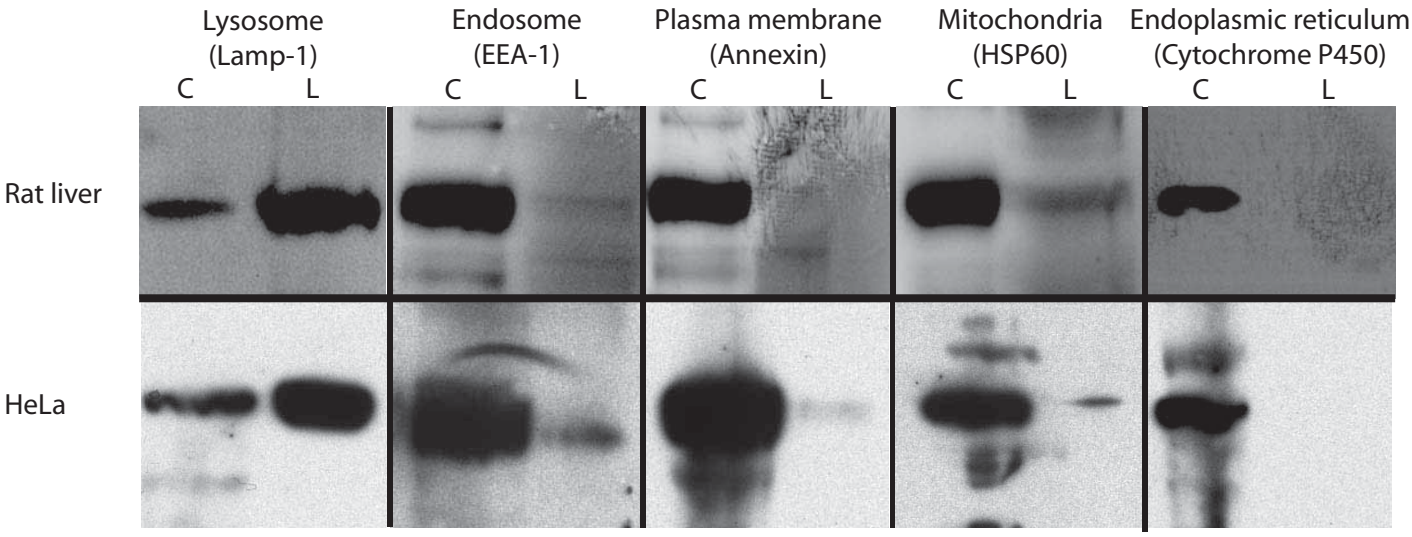

Supplemental Figure 1: Specific enrichment of lysosomal markers from rat liver and from HeLa cells.

Western blots of organelle marker proteins in the preparations used in this work. Equal amounts of total protein from either rat liver or HeLa cell crude homogenates (C) or lysosomes (L) were loaded on reducing gels and blotted with antibodies specific for organelle markers as indicated. Lysosomal fractions were highly enriched for lysosomal markers and were depleted for markers of other subcellular membrane components.

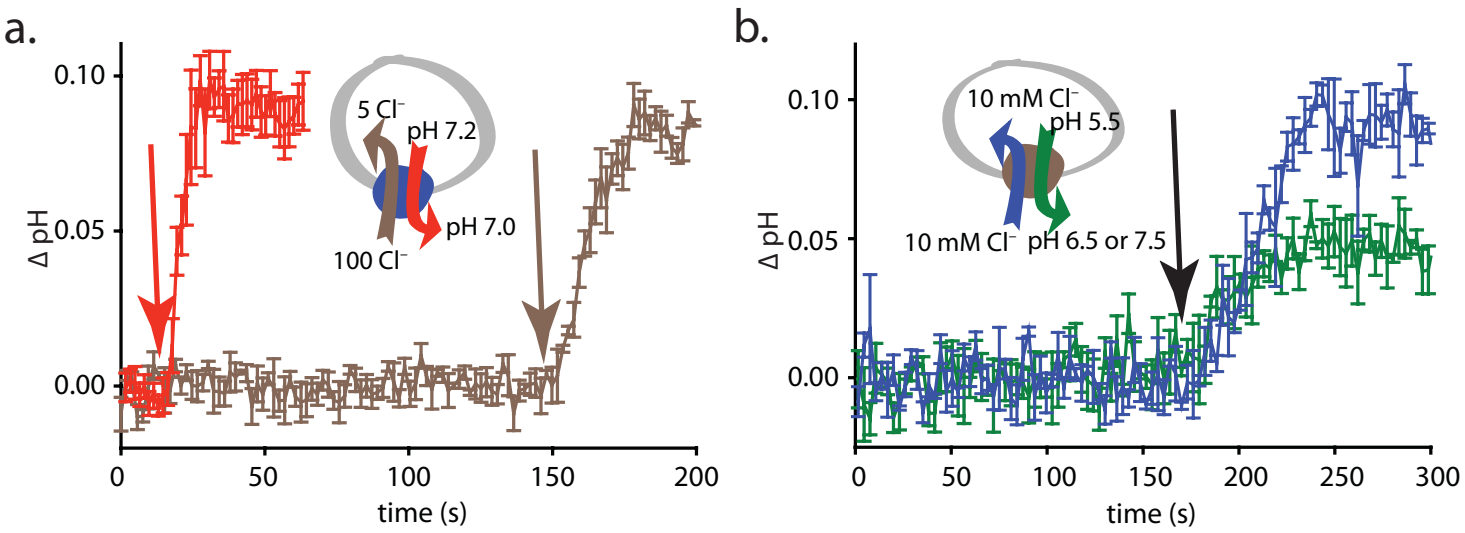

Supplemental Figure 2: Internal lysosomal pH is stable until valinomycin addition.
a. The internal lysosomal pH, measured in rat liver lysosomes with BCECF, is stable for at least 150 s (brown trace) until valinomycin is added (brown arrow). Conditions are identical to those used in Figure 2 (pH 7.2 in/7.0 out, 0 mV, for comparison, red trace represents the same data shown in the red trace in Figure 2a).
b. pH stability in conditions close to those of experiments in Figure 3. The pH also remains stable in lysosomes at lower pH and with a larger gradient [pH 5.5 in/6.5 (green trace) or 7.5 out (blue trace)]. The higher pH used here is in the linear range of BCECF (see Supplemtal Figure 3). Again in these experiments the internal pH was stable over ~150 s, but changes upon initiation of antiport by valinomycin addition (black arrow). Aside from the pH, solutions are essentially identical to those from Figure 3 at 0 mV. In both panels, data values represent mean ± s.e.m for (n = 3).

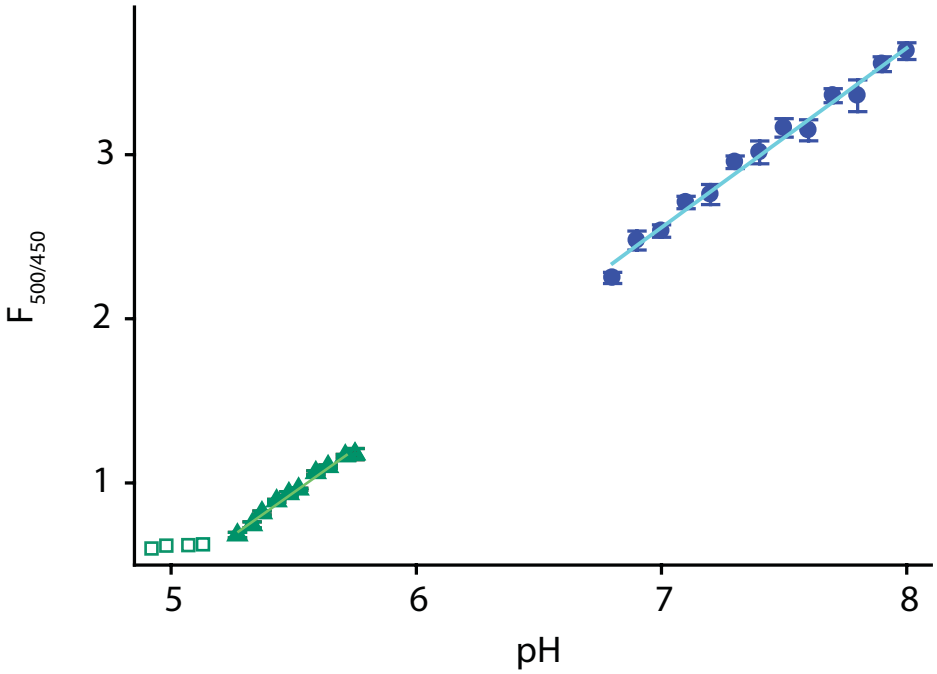

Supplemental Figure 3: Calibration and linearity of BCECF fluorescence.
BCECF fluorescence emission ratios ($F_{500/450}$: emission at 535 nm with excitation at 500 nm ÷ emission at 535 nm with excitation at 450 nm) were measured as a function of pH for BCECF free in solution in the pH ranges of interest for our transport experiments. Though the ratios are linear and sensitive to small changes in pH above pH 5.25 (blue circles, green triangles), their sensitivity drops dramatically below pH 5.25 (open squares). For data between pH 6.8 and 8.0, the ratios are fit by the equation: $F_{450/500}$=1.094 × pH – 5.10 (R=0.986, light blue line); for data between pH 5.3 and 5.8 the data are fit by the equation $F_{450/500}$ = 1.054 × pH – 4.85 (R=0.989, light green line); these equations are used to determine the pH values plotted in Figure 2 and in Supplemental Figure 2. Solutions included 5 μM BCECF, 10 mM KCl, 90 mM $NaCH_3SO_3$, and 20 mM citrate (pH 4.9-5.8, green symbols) or 10 mM KCl , 20 mM HEPES (pH 6.8-8.0, blue symbols).

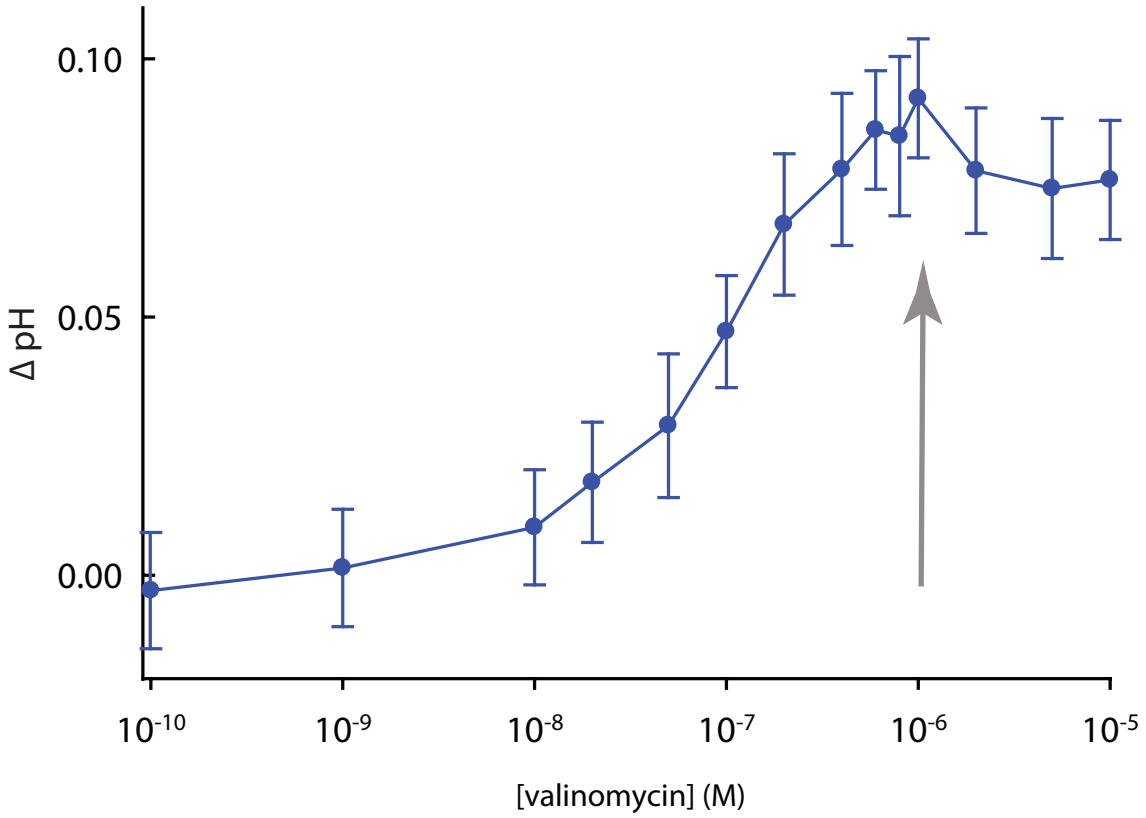

Supplemental Figure 4: Determination of an effective valinomycin concentration. For valinomycin to set the membrane potential to $E_{K'}$ it must make the membrane overwhelmingly permeable to K^+ over other ions. To determine an appropriate concentration for our experiments we performed control experiments using BCECF to monitor pH changes in varying concentrations of valinomycin in rat lysosomes under the conditions described in Figure 2. At low concentrations, the ionophore should induce a small K^+ permeability and minimally shift the membrane voltage from its preestablished value (which is $E_{transporter}$). As the valinomycin concentration is increased it will permeablize the membrane more and shift the potential closer to $E_{K'}$ thereby causing a larger H^+ flux. Once enough val. Is added to set the membrane voltage to $E_{K'}$ further additions will cause no additional pH change. Lysosomes were prepared as above and valinomycin was added incrementally while monitoring lysosomal pH, starting a trace concentration (10^{-10} M) and increasing until no further changes in pH were observed (~10^{-6} M). At such concentrations, the membrane potential must asymptotically approach the equilibrium potential of K^+. The grey arrow indicates the valinomycin concentration used for this work.

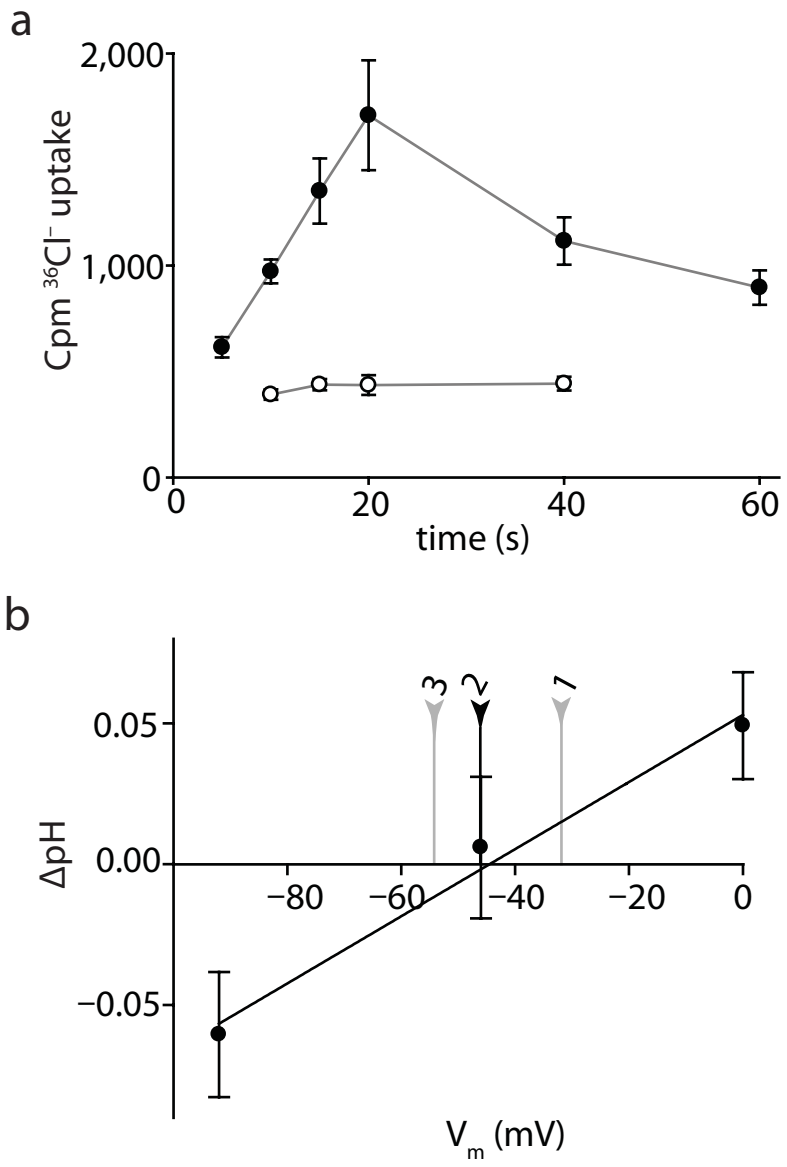

Supplemental Figure 5. Transport properties of WT HeLa lysosomes.
a. Concentrative $^{36}Cl^-$ uptake. HeLa lysosomes containing 500 mM Cl^-, pH 4 were diluted into a solution containing 2 mM $^{36}Cl^-$, pH 4 at t = 0 without (filled symbols) or with (open symbols) valinomycin. At the indicated times, uptake was terminated and retained radioactivity measured. n=6 ± s.e.m.
b. Cl^--coupled H^+ transport. HeLa lysosomes contained 5 mM Cl^- and 200 μM BCECF at pH 7.2 and were diluted into an external buffer containing 100 mM Cl^- and 5 mM K^+ at pH 7. $[K^+]_{in}$ was varied to set E_K at 0 mV (5 mM), -46 mV (30.5 mM), or -92 mV (200 mM). BCECF fluorescence emission was monitored and pH calculated as in Figure 2. ΔpH was calculated at each voltage by taking the difference of the mean steady state pH before and after initiating H^+ flux with valinomycin (circles). Arrows indicate predicted reversal potentials for a 3, 2, and 1 Cl^-:1H^+ antiport stoichiometries. n = 5 ± s.e.m. Data were fit by linear regression (black line, $R^2 = 0.9854$, x-intercept = -44 mV). Though the scatter of the HeLa data precludes precise analysis, these results are consistent with measurements made on rat lysosomes, suggesting that HeLa lysosomes also contain a 2Cl^-:1H^+ antiporter. Combined with the results in Figure 4 these data support the contention that the HeLa lysosome anion pathway is identical to that observed in rat lysosomes.

Methods

Lysosomal enrichment from rat liver and HeLa cell culture

Saline-perfused livers from overnight-fasted Sprague-Dawley rats were dissected, minced, and homogenized using 3 strokes of a motorized Potter-Elvehjem homogenizer running at ~3000 rpm. Lysosomes were isolated by differential centrifugation on a self-generated Percoll gradient[7] (40% (v/v) starting concentration), and Percoll removed by centrifugation at 100,000 x g for 1 hr. Lysosomal fractions were identified using enzyme assays or Western blots with α-LAMP-1 antibody . Total lysosomal protein was measured using BCA assays (Pierce) and lysosomes were stored at -80° C.

Concentrative and proton-driven $^{36}Cl^-$ uptake

Samples containing 100 μg total lysosomal protein were loaded by freeze/thaw-sonication in the desired internal buffer (see below). For anion-dependence experiments internal KCl was replaced with KBr, KNO_3, KI or KCH_3SO_3. External solutions were exchanged by passage through sephadex G-50 columns equilibrated in external buffer (see below). Concentrative uptake was initiated by adding $^{36}Cl^-$ to the outside buffer; H^+-driven $^{36}Cl^-$ uptake was initiated by addition of 1 μM valinomycin. Control experiments reveal that this valinomycin concentration is sufficient to set the lysosome membrane potential to E_K, the potassium equilibrium potential (Supplemental Figure 4). Uptake reactions were terminated by binding to nitrocellulose filters followed by vacuum filtration and washing to remove external radioactivity. Retained radioactivity was measured by liquid scintillation.

Fluorescence measurements of H^+ and Cl^- flux

Lysosomes were prepared as described for the uptake assays. 200 μM BCECF or SPQ was trapped in lysosomes along with the desired internal solution (see below) by freeze-thaw/sonication; external solutions (see below) were replaced as above by passage through sephadex G-50 columns. Lysosomes were introduced to a Jobyn-Yvon Fluoromax-3 fluorimeter, constantly stirred, and held at 22°C for the duration of the experiment using a Peltier temperature controller. In the proton flux experiments, BCECF excitation wavelengths alternated between 500nm and 450nm while measuring emission at 535 nm. For Cl^- flux, SPQ was excited at 344 nm with emission spectra collected from 420-460nm. In both sets of experiments, transport was initiated by adding 1μM valinomycin to the fluorescence cuvette. pH

values were determined by calculating the ratio of BCECF emission from 500 nm excitation/450 nm excitation (R). This value was converted to pH using the equation pH=(R+5.1)/1.1 which was determined by calibrating the fluorophore in the internal buffer used for these experiments.

Solutions used for flux measurements:

Figure 1: $^{36}Cl^-$ uptake measurements:

1a, Concentrative uptake: external solutions contained 2 mM $Na^{36}Cl$, 498 mM KCH_3SO_3, 1 mM $NaVO_3$, and 20 mM HEPES (pH 7.0) or 20 mM citrate (pH 4.0 or pH 5.5); internal solutions contained 500 mM KCl and 20 mM HEPES (pH 7.0) or 20 mM citrate (pH 4.0 or pH 5.5).

1b Anion dependence: as above, but replacing KCl with KNO_3, KBr, KI or KCH_3SO_3 as indicated.

1c H^+-driven $^{36}Cl^-$ uptake: external solutions contained 5 mM $Na^{36}Cl$, 10 mM KCH_3SO_3, 1 mM $NaVO_3$, 1 μM valinomycin, and 20 mM HEPES pH 7.0; internal solutions contained 5 mM NaCl, 10 mM KCH_3SO_3, and 20 mM citrate pH 4.0.

Figure 2a, 2b: H^+-reversal potential measurements:

External solutions all contained 5 mM KCl, 20 mM HEPES pH 7.0, and 1 mM $NaVO_3$. Internal solutions all contained 5 mM KCl, 20 mM HEPES, pH 7.2, 200 μM BCECF. In addition internal and external solutions contained (in mM):

Voltage (mV)	NaCl out	$NaCH_3SO_3$ out	KCH_3SO_3 in	$NaCH_3SO_3$ in
0 mV	95	0	0	96
-32 mV	95	0	12.75	83.5
-46 mV	95	0	25.6	69.5
-54 mV	95	0	37.5	58.5
-93 mV	95	99	195	0

Figure 2c, 2d: Cl^--reversal potential measurements:

External Solutions all contained: 10 mM KCl, 20 mM citrate pH 6.0, 1 mM $NaVO_3$. Internal solutions all contained: 10 mM KCl, 20 mM citrate pH 4.75, 200 μM SPQ. In addition internal and external solutions contained (in mM):

Voltage (mV)	KCH_3SO_3 out	$NaCH_3SO_3$ out	KCH_3SO_3 in	$NaCH_3SO_3$ in
-59	0	89	90	0
-36	13.7	75.3	90	0
-24	28.3	60.7	90	0
-18	38.7	50.3	90	0
0	90	0	90	0
+20	90	0	35.5	50.5

Cell culture and siRNA mediated knockdown of ClC-7

HeLa cells were grown in Dulbecco's modified Eagle's medium with 10% fetal bovine serum and maintained in a humidified 37°C incubator with 5% CO_2. ClC-7 pre-designed siRNA(Ambion 104370 and 145731) and Silencer negative control siRNA (Ambion) were used to knock down the transcript. 10 x 500 cm^2 flasks were seeded with sufficient cells to generate a harvest of ~6g. For single transfection experiments, cells were transfected with 46 nM siRNA [ClC-7 pre-designed siRNA, Ambion 104370 or 145731; or Silencer negative control siRNA (Ambion)] complexed with siPORT NeoFx (Ambion) and collected 72 hours after transfection. For double-transfection experiments, cells were transfected as above (with siRNA 145731 or with Silencer negative control) incubated for 72 hours, retransfected with the same siRNA, and incubated for another 72 hours before collection. Collected cells were lysed using nitrogen cavitation[22] and lysosomes prepared as above. Cells for imaging experiments were treated identically but were grown on glass coverslips.

Imaging of HeLa cells

Cells were imaged using an LSM 510 (Carl Zeiss Inc.) confocal microscope with a 63x, 1.4 NA objective. Before imaging cells were transferred to phenol-red free DMEM buffered with HEPES. For live cell imaging, 50 nM LysoTracker Green was added to the bathing medium and incubated for 10 min; fluorescence was excited using a 488 nm laser. For immunostaining, cells were fixed with 4% paraformaldehyde, washed with PBS, incubated with anti-LAMP-1 primary antibody and an Alexa-546 conjugated secondary (Invitrogen), and

imaged with the same system, using a 543 nm laser for excitation. All imaging conditions were kept identical to facilitate quantitative comparison; after collection images were manipulated identically for display. Quantitative analysis was performed with Metamorph software (Molecular Devices). Confocal images through a field of cells were summed to yield an image reflecting the total LysoTracker staining intensity through the thickness of the cells; all cells completely contained in the field were manually outlined to define regions of interest for measurement. A threshold value representing the background staining of a cell-free area of the stack was subtracted from each pixel of the summed image and the total intensity of each cell determined by integrating the super-threshold values of all pixels in the region.

Western blots

The relative enrichment or depletion of markers for liver organelles and CLCs in our lysosomal preparation was determined using Western blots. Primary antibodies (unless noted, all antibodies were polyclonal, and affinity purified) were: anti-ClC-7 (Alpha Diagnostics), anti-ClC-2 (Santa Cruz), anti-ClC-3 (which crossreacts with ClC's -4 and -5; Santa Cruz), anti-ClC-6 (Santa Cruz), monoclonal anti-Lamp-1 (Stressgen), anti-annexin (BD Transduction), anti-Hsp-60 (BD), anti-EEA-1 (BD), anti-ERp57 (BD). HRP IgG secondary antibodies were purchased from Zymed. PVDF membranes were blocked with 3% BSA in TBS-T, incubated in primary antibody overnight, washed, and incubated in secondary antibody for 30 minutes. Blots were visualized using chemiluminescence (SuperSignal®, Pierce) and imaged using a UVP bio imaging system or film. Blot films were digitized using a GS-800 densitometer (BioRad).

Data analysis and statistical methods

For $^{36}Cl^-$ uptake experiments, data points are the means of 3-11 experiments and are plotted ± s.e.m.

For experiments with BCECF, pH was calculated as above for each time point. A series of measurements at steady state, either before or after addition of valinomycin, were averaged across several experiments (~15 points/experiment x 4-8 experiments) and s.e.m. determined. For figure 2b, ΔpH was determined as the difference between steady-state pH after and before valinomycin addition and the error bars indicate:

$$SEM_{\Delta pH} = \sqrt{SEM_{after}^2 + SEM_{before}^2}$$

For experiments with SPQ, spectra were collected before and after valinomycin addition for 4-6 experiments. Within each experiment, spectra were normalized to the fluorescence emission at 440nm before valinomycin. Differences between spectra before and after valinomycin addition were calculated and averaged, and then integrated between 428 and 456 nm:

$$\int_{428}^{456} \Delta F d\lambda = \sum_{428}^{456} \Delta F \bullet \Delta\lambda$$

Errors for the integral were calculated as follows:

$$SEM_{integral} = \sqrt{\sum_{\lambda} (SEM_{\lambda} \bullet \Delta\lambda)^2}$$

For Figure 4a, uptake measurements were performed and analyzed using the methods described for the experiments in Figure 1c. To calculate the % reduction in function caused by siRNA, mean background levels of uptake at 20s (+valinomycin) were subtracted from the mean experimental values and % reduction calculated. S.e.m. for the difference was calculated as the square root of the sum of the squared s.e.m.s. Significance was determined using a two-tailed Student's t-test.